CrossMark

TG–MS study on the kinetics and mechanism of thermal decomposition of copper ethylamine chromate, a new precursor for copper chromite catalyst

Sanoop Paulose[1] · Deepthi Thomas[1] · T. Jayalatha[1] · R. Rajeev[1] · Benny K. George[1]

Abstract Copper chromite is a well-known burn rate modifier for the combustion of composite solid propellants. In this study, basic copper ethylamine chromate (CEC), a new precursor for copper chromite catalyst, was synthesized by precipitation method. The thermal decomposition of the precursor was followed by thermogravimetry–mass spectroscopy (TG–MS) and X-ray diffraction techniques and compared with that of copper ammonium chromate, a conventional precursor for copper chromite catalyst. TG–MS analysis for the decomposition of CEC revealed that the decomposition starts with the liberation of ethylamine. The change in enthalpy for the decomposition reaction of copper ethylamine chromate was higher than that of copper ammonium chromate due to the oxidation of ethyl group. The reducing atmosphere created by the presence of carbon during the decomposition of CEC produced a mixture of Cu, $CuCr_2O_4$, $CuCrO_2$ and CuO, while the oxidizing atmosphere of copper ammonium chromate produced a mixture of $CuCr_2O_4$ and CuO. Mechanistic study based on Criado and Coats–Redfern methods showed that CEC follows random nucleation (F1) mechanism as the rate-determining step for the thermal decomposition process.

Keywords Copper ethylamine chromate · Copper chromite · Burn rate modifier · Thermal decomposition

✉ R. Rajeev
arerajeev@gmail.com

Sanoop Paulose
sanoop_ap@vssc.gov.in

[1] Analytical and Spectroscopy Division, Analytical, Spectroscopy and Ceramics Group Propellants, Polymers, Chemicals and Materials Entity, Vikram Sarabhai Space Centre, Trivandrum 695022, India

Introduction

Composite solid propellants (CSP) are the major source of chemical energy for the propulsion of space vehicles and missiles. CSP are heterogeneous mixtures consisting of an oxidizer, usually ammonium perchlorate (AP), a metallic fuel like aluminium powder and a fuel-cum-binder, generally hydroxyl-terminated polybutadiene. In addition, they contain curing agents, plasticizers, bonding agents and deoxidizers for improving their mechanical and storage properties and burn rate modifiers for improving burning rate. Being complex mixtures, their combustion behaviour is quite complex. Studies on various kinds of catalysts and additives for controlling the burn rate of CSP and the thermal decomposition kinetics of its oxidizer, AP, were well documented in the literature [1–6].

The most commonly used and effective burn rate modifiers are transition metal oxides (TMO), especially copper chromite and iron oxide [7]. The catalytic system of copper chromite, $CuO.CuCr_2O_4$, first reported by 'Adkins', has wide commercial application as catalyst for chemical reactions such as hydrogenation, dehydrogenation, oxidation and alkylation [8]. In addition to versatile commercial applications as a catalyst, copper chromite finds application as a ballistic modifier for composite solid propellants [9]. Copper chromite accelerates the thermal decomposition of AP, thereby increasing the burn rate of propellant combustion [10, 11]. In AP decomposition, copper chromite acts as heterogeneous catalyst, facilitating the decomposition of perchlorate/perchloric acid formed on the catalyst surface as well as the oxidation of ammonia [12].

The catalytic activity of copper chromite depends on its chemical nature, particle size and surface area. The chemical and physical characteristics of copper chromite catalyst vary according to the method of preparation [13, 14]. The type of

🙂 Springer

precipitating agent used for the preparation of precursor to copper chromite, pH of the precipitating medium, thermal decomposition temperature, etc. can affect the catalytic activity of copper chromite.

In this work, we are focusing on the kinetics and mechanism of thermal decomposition of basic copper ethylamine chromate (CEC), a new precursor for copper chromite catalyst. The synthesis, characterization and application of CEC were already reported [15]. TG–MS and XRD techniques were employed to evaluate thermal decomposition and to identify the composition of volatile and non-volatile products. Kinetic parameters such as activation energy and pre-exponential factor were derived from the TG data using multiple heating rate methods, viz. Kissinger–Akahira–Sunose (KAS) and Flynn–Wall–Ozawa (FWO) [16–21]. Criado method was employed to find out a reaction mechanism for the thermal decomposition of precursor [22, 23]. The results were compared with the thermal decomposition of copper ammonium chromate (CAC), the precursor for conventional copper chromite catalyst [24–29].

Methodology

Materials

Analytical-grade reagents, viz. copper nitrate trihydrate, ammonium dichromate, ethylamine (70 % aqueous solution) and ammonia solution (25 %), from SD Fine Chemicals, India, and chromium trioxide trihydrate from SRL Chemical, India, were used for the synthesis of catalysts.

Preparation of precursors and copper chromite catalysts

The precursor, basic copper ethylamine chromate was synthesized according to a previously reported precipitation method [15]. Different batches of the precursors were then heated in a muffle furnace at 598, 773, 973 and 1123 K for 1 h under nitrogen atmosphere. Similarly, the conventional basic copper ammonium chromate was prepared from cupric nitrate (240 g in 250 mL of water) and ammonium dichromate (126 g in 100 mL of water) using ammonia as the precipitating agent. Different batches of CAC were then heated in a muffle furnace for 1 h at 623, 773 and 973 K (23, 24 and 26) to obtain respective samples. CEC and CAC samples heated at different temperatures are subjected to XRD analysis.

Characterization

Perkin Elmer Pyris 1 TGA thermogravimetric analyzer clubbed with a Perkin Elmer Clarus SQ8T mass

spectrometer was used for the TG–MS study. The crystal phase of the precursors and non-volatile decomposition products were identified by Bruker D8-Discover powder X-ray diffraction spectrometer using CuKα radiation (1.5418 A°) at a scan rate of 2.5° min^{-1}. Simultaneous TG–DSC, TA Instruments Q600, was employed for evaluating the thermal decomposition of the precursors. In all the TG–DSC experiments, a sample mass of 5 ± 1 mg in platinum sample cup was used and furnace was purged with ultrapure nitrogen gas at a flow rate of 100 mL min^{-1}. For evaluating the kinetic parameters, TG analysis of the precursor was carried out at variable heating rates (5, 10, 20 and 40 K min^{-1}).

Thermal decomposition kinetics

Kinetic parameters for the thermal decomposition of CEC and CAC were calculated using two isoconversional multiple heating rate methods, viz. Kissinger–Akahira–Sunose (KAS) and Flynn–Wall–Ozawa (FWO) [16–21]. Both KAS and FWO methods are suitable for the determination of the kinetic parameters without any prior knowledge of the reaction mechanisms.

KAS method is based on the following equation

$$\ln \frac{\beta}{T_\alpha^2} = \ln \left[\frac{AR}{g(\alpha)E_\alpha} \right] - \frac{E_\alpha}{RT_\alpha} \qquad (1)$$

where β is the heating rate, T_α is the temperature in Kelvin corresponding to a fixed degree of conversion, α, A is the pre-exponential factor, R is the gas constant, E_α is the activation energy at a given degree of conversion and $g(\alpha)$ is the integral form of kinetic model function. E_α for a given degree of conversion is obtained from the slope of the linear fit of the plot $\ln \frac{\beta}{T_\alpha^2}$ versus $1/T_\alpha$.

The isoconversional FWO method is represented by the following equation

$$\log \beta = \log \left[\frac{AE_\alpha}{g(\alpha)R} \right] - 2.315 - b \frac{E_\alpha}{RT_\alpha} \qquad (2)$$

where 'b' is an approximation constant [21]. A plot of log (β) against $1/T_\alpha$ gives a straight line with slope d (log β)/d ($1/T_\alpha$). The E_α of the reaction is calculated using the equation

$$E_\alpha = - \left[\frac{R}{b} \right] \frac{d \log \beta}{d \left(\frac{1}{T_\alpha} \right)} \qquad (3)$$

The E_α values obtained from FWO method are approximate and hence require refining as per the method given by ASTM E 1641 [21]. The activation energy values obtained by both methods are used to determine the corresponding pre-exponential factors, A, using the equation,

$$A = \frac{\beta E_\alpha e^{E_a/RT\alpha}}{RT_\alpha^2} \tag{4}$$

Several kinetic equations have been proposed and used during the last decades for the description of solid-state reactions such as random nucleation, nucleation and growth, diffusion and phase boundary controlled reactions [22]. As given in Table 1, the algebraic expressions that represent the theoretical mechanisms are separated into four groups, viz., D_n, F_n, A_n and R_n, representing nuclei formation processes for the propagation of thermal degradation, diffusion processes that are related to the heat transfer capacity along the material structure, random nucleation and reaction mechanisms controlled by the phase boundary reactions.

All kinetic studies assume that the isothermal rate of conversion, $d\alpha/dt$, is a linear function of a temperature-dependent rate constant, k, and a temperature-independent function of the conversion, α, that is:

$$\frac{d(\alpha)}{dt} = k(T)f(\alpha) \tag{5}$$

If a reaction is proven to be isokinetic over the range of temperature studied, Arrhenius equation can be applied to Eq. (5) to give

$$\frac{d(\alpha)}{dt} = A\exp\left[-\frac{E_a}{RT}\right]f(\alpha) \tag{6}$$

where A is frequency factor/pre-exponential factor (s^{-1}), E_a is activation energy (kJ mol^{-1}), R is universal gas constant (8.314 J mol^{-1} K^{-1}) and T is absolute temperature (K).

In non-isothermal condition of constant heating rate $= dT/dt$, the conversion degree can be analysed on a function of temperature and the Eq. (6) becomes

$$\frac{d(\alpha)}{dT} = \frac{A}{\beta}\exp\left[-\frac{E_a}{RT}\right]f(\alpha) \tag{7}$$

To find out a solution for this non-isothermal kinetic equation, Coats–Redfern used the integral form of the rate law, which utilized the asymptotic series expansion for approximating the temperature integral, producing [30]:

$$\ln\frac{g(\alpha)}{T^2} = \ln\left[\frac{AR}{\beta E_a}\left\{1 - \left(\frac{2RT}{E_a}\right)\right\}\right] - \frac{E_a}{RT} \tag{8}$$

This equation was used to obtain the master curves by replacing $g(\alpha)$ with corresponding models listed in Table 1. Plotting $\ln\frac{g(\alpha)}{T^2}$ versus $1/T$ gives a linear fit with a slope, from which E_a can be calculated. The model that gives the best linear fit and comparable E_a value with that obtained by model free methods is chosen as the preferred one to explain the reaction mechanism.

Results and discussion

First-stage thermal decomposition of CEC and CAC (423–598 K)

The TG–DSC curves for the thermal decomposition of CEC and CAC are shown in Fig. 1a, b, respectively, and the phenomenological data corresponding to each stage of decomposition are given in Table 2. Figure 1a, b shows that the thermal decomposition behaviour of CEC is different from that of CAC. CEC shows four stages of mass loss, while CAC shows only three stages. In both cases, except for the exothermic first-stage decomposition, all the other stages are endothermic in nature. From Fig. 1a, b, it

Table 1 Algebraic expressions for the frequently used mechanisms of solid-state decomposition processes

Function	$g(\alpha)$	$F(\alpha)$	Rate-controlling process
D_1	α^2	$\frac{1}{2}(\alpha)$	One-dimensional diffusion
D_2	$(1-\alpha)\ln(1-\alpha) + \alpha$	$-\ln(1-\alpha)^{-1}$	Two-dimensional diffusion, cylindrical symmetry
D_3	$[1-(1-\alpha)^{1/3}]^2$	$\{(3/2)(1-(1-\alpha)^{1/3})^{-1}(1-\alpha)\}^{2/3}$	Three-dimensional diffusion, spherical symmetry; Jander equation
D_4	$(1-2/3\alpha) - (1-\alpha)^2/3)$	$(3/2)(1-(1-\alpha)^{1/3})^{-1}$	Three-dimensional diffusion, spherical symmetry; Ginstling–Braunshtein equation
F_1	$-\ln(1-\alpha)$	$(1-\alpha)$	Random nucleation, one nucleus on each particle
F_2	$1/(1-\alpha)$	$(1-\alpha)^2$	Random nucleation, two nuclei on each particle
F_3	$1/(1-\alpha)^2$	$(1/2)(1-\alpha)^3$	Random nucleation, three nuclei on each particle
A_2	$-\ln\{(1-\alpha)\}^{1/2}$	$2(1-\alpha) - \ln\{(1-\alpha)\}^{1/2}$	Random nucleation, Avrami equation I
A_3	$-\ln\{(1-\alpha)\}^{1/3}$	$3(1-\alpha) - \ln\{(1-\alpha)\}^{2/3}$	Random nucleation, Avrami equation II
A_4	$-\ln\{(1-\alpha)\}^{1/4}$	$4(1-\alpha) - \ln\{(1-\alpha)\}^{3/4}$	Random nucleation, Avrami equation III
R_1	α	1	Phase boundary reaction(1D movement)
R_2	$(1-\alpha)^{1/2}$	$2(1-\alpha)^{1/2}$	Phase boundary reaction, cylindrical symmetry
R_3	$(1-\alpha)^{1/3}$	$3(1-\alpha)^{2/3}$	Phase boundary reaction, spherical symmetry
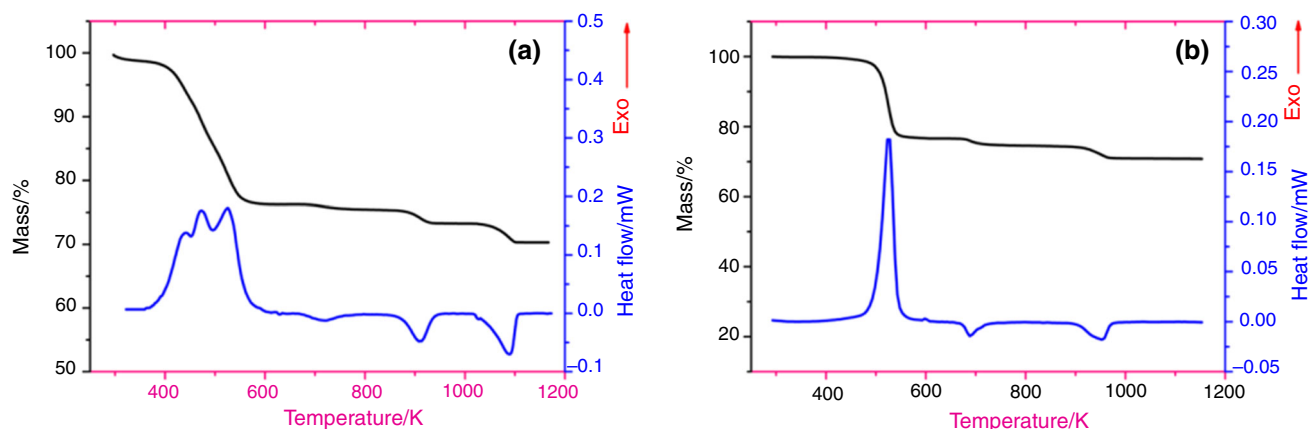
Fig. 1 TG and DSC curves for the thermal decomposition of CEC and CAC

Table 2 Phenomenological data for thermal decomposition of CEC and CAC

Sample	First stage			Second stage			Third stage			Fourth stage		
	T_i/K	T_s/K	T_f/K	T_i/K	T_s/°C	T_f/K	T_i/K	T_s/K	T_f/K	T_i/K	T_s/K	T_f/K
CEC	423	473	598	683	717	768	849	908	953	1023	1088	1123
	$\Delta m = 24.1$ %			$\Delta m = 0.72$ %			$\Delta m = 2.2$ %			$\Delta m = 3.0$ %		
	Exo			Endo			Endo			Endo		
CAC	473	534	598	673	698	773	973	958	9	Nil		
	$\Delta m = 23.1$ %			$\Delta m = 1.8$ %			$\Delta m = 3.4$ %			Nil		
	Exo			Endo			Endo			Nil		

Δm = Mass loss

is evident that the first-stage decomposition of CEC starts at a lower temperature than that of CAC which may be due to the instability of the complex containing bulky ethylamine group. DSC measurements of first-stage decomposition of CEC showed an overall ΔH of 570 J g^{-1} which was higher than the ΔH for the first-stage decomposition of CAC ($\Delta H = 260$ J g^{-1}), indicating the higher exothermicity of the reaction.

Total ion chromatograms for various volatile products obtained from TG–MS analysis of CEC and CAC during the thermal decomposition from 300 to 1173 K are shown in Fig. 2a, b, respectively. Total ion chromatograms of CEC (Fig. 2a) indicate that the reaction starts with the evolution of $C_2H_5NH_2$ and NH_3 which is immediately followed by the evolution of H_2O and CO_2, indicating the oxidation of initial volatile products. However, CAC shows the presence of H_2O, NH_3 and nitrous oxide (N_2O) during the first-stage thermal decomposition (Fig. 2b) with H_2O and NH_3 as the initial products followed by N_2O.

Figure 3 represents the XRD of CEC and CAC as prepared. The peak positions and relative intensities of CAC agree well with the XRD patterns of copper ammonium chromate with the formula Cu (OH) (NH$_4$) CrO$_4$ ($2\theta = 26.9$, 30.1, 35.1) [26]. Even though X-ray

diffractogram of the CEC is almost matching with CAC at some intervals, it shows more number of sharp peaks than CAC. The presence of peaks at 2θ values of 20.9, 28.2, 32.2 and 41.1 may be specific for the structure of CEC along with the standard peaks at 26.9, 30.1 and 35.1° of CAC.

The X-ray diffractograms of CEC and CAC subjected to heating at 598 K for 1 h in a muffle furnace under nitrogen atmosphere are shown in Fig. 4a, b, respectively. They show broad and weak peaks, indicating the amorphous nature of the products with respect to that of precursors. For CEC heated at 598 K for 1 h (Fig. 4a), all the diffraction peaks can be readily indexed to Cu (JCPDS No. 00-004-0836), CuCrO$_2$ (JCPDS No.04-010-3330), CuO (JCPDS No. 00-048-1548) and CuCr$_2$O$_4$ (JCPDS No. 00-005-0657) phases, whereas Fig. 4b shows the presence of CuCr$_2$O$_4$ and CuO phases only. The volatile reaction products from the thermal decomposition of CEC and CAC were identified, and the corresponding mass spectra are given in Fig. 5a, b, respectively. Ethylamine ($C_2H_5NH_2$), ammonia (NH_3), water (H_2O) and carbon dioxide (CO_2) are the volatile products identified by MS during the first-stage thermal decomposition of CEC. The absence of oxygen or oxidizing species like N_2O and the presence of
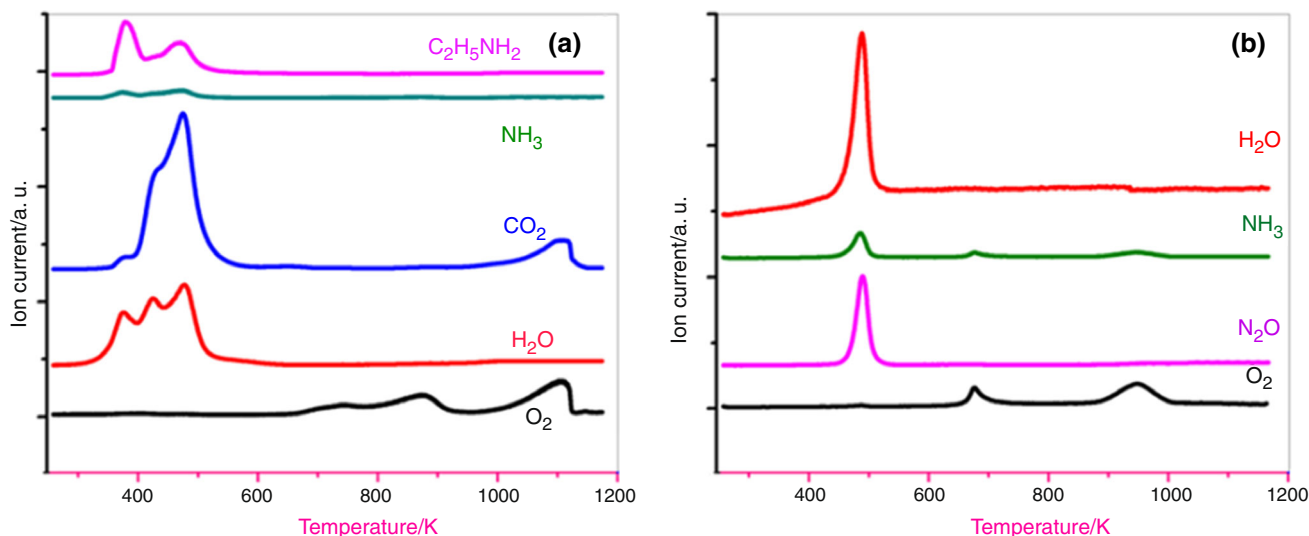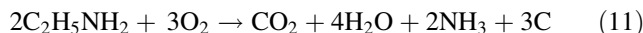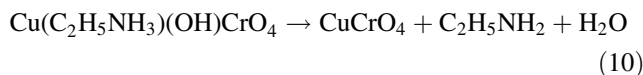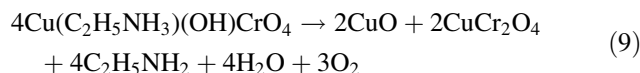
Fig. 2 Total ion chromatograms obtained from TG–MS of CEC and CAC decomposition

CO_2 among the volatile products of first-stage decomposition of CEC as well as the presence of carbon and metallic copper in the non-volatile residue confirmed that incomplete oxidation has been taken place during this stage and the prevailing atmosphere was reducing in nature.

In contrast, the total ion chromatograms and mass spectrum (Fig. 2b and 5b) of CAC show the presence of H_2O, NH_3 and nitrous oxide (N_2O) during the first-stage thermal decomposition. The formation of N_2O indicates the presence of excess oxygen, which oxidizes NH_3 to H_2O and N_2O. A closer look at the total ion chromatograms (Fig. 2b) shows that H_2O and NH_3 are the initial products which are followed by the appearance of N_2O, an oxidation product at high temperature.

Based on these observations, the possible reactions taking place during the first-stage decomposition of CEC are

$$4Cu(C_2H_5NH_3)(OH)CrO_4 \rightarrow 2CuO + 2CuCr_2O_4 \\ + 4C_2H_5NH_2 + 4H_2O + 3O_2 \tag{9}$$

$$Cu(C_2H_5NH_3)(OH)CrO_4 \rightarrow CuCrO_4 + C_2H_5NH_2 + H_2O \tag{10}$$

$$2C_2H_5NH_2 + 3O_2 \rightarrow CO_2 + 4H_2O + 2NH_3 + 3C \tag{11}$$

$$2CuO + 2CuCr_2O_4 + C \rightarrow 4CuCrO_2 + CO_2 \tag{12}$$

$$2CuO + C \rightarrow 2Cu + CO_2. \tag{13}$$

Second-stage thermal decomposition (673–773 K)

A second-stage mass loss is observed in the curves (Fig. 1a, b) of CEC and CAC from 673 to 773 K. Reactions are endothermic in nature for both cases, but the mass loss for CEC is almost half (0.7 %) of that in CAC (1.8 %) (Table 2). The MS analysis (Fig. 6) showed that oxygen is the only volatile product evolved during this stage, and XRD of CEC (Fig. 7) heated at 773 K shows the presence of Cu, CuO, $CuCrO_2$ and $CuCr_2O_4$ phases.

It was reported that the second-stage mass loss in CAC is due to the decomposition of $CuCrO_4$, which was formed during the first-stage decomposition [26]. Similarly, $CuCrO_4$ is formed during the decomposition of CEC also (Eq. 10). However, the reducing environment during CEC decomposition prevents the formation of more quantities of $CuCrO_4$ which is basically an oxidized form of Cu and Cr. This was reflected in the observed lower mass loss for the second-stage decomposition of CEC than that of CAC.
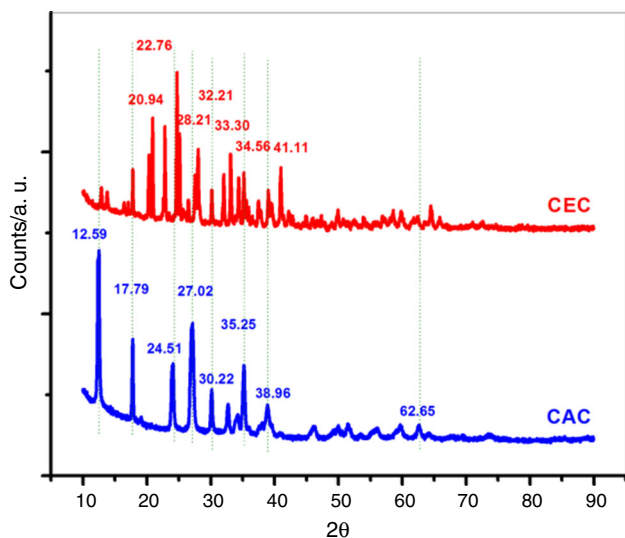
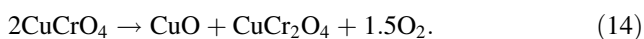**Fig. 3** X-ray diffractograms of CEC and CAC
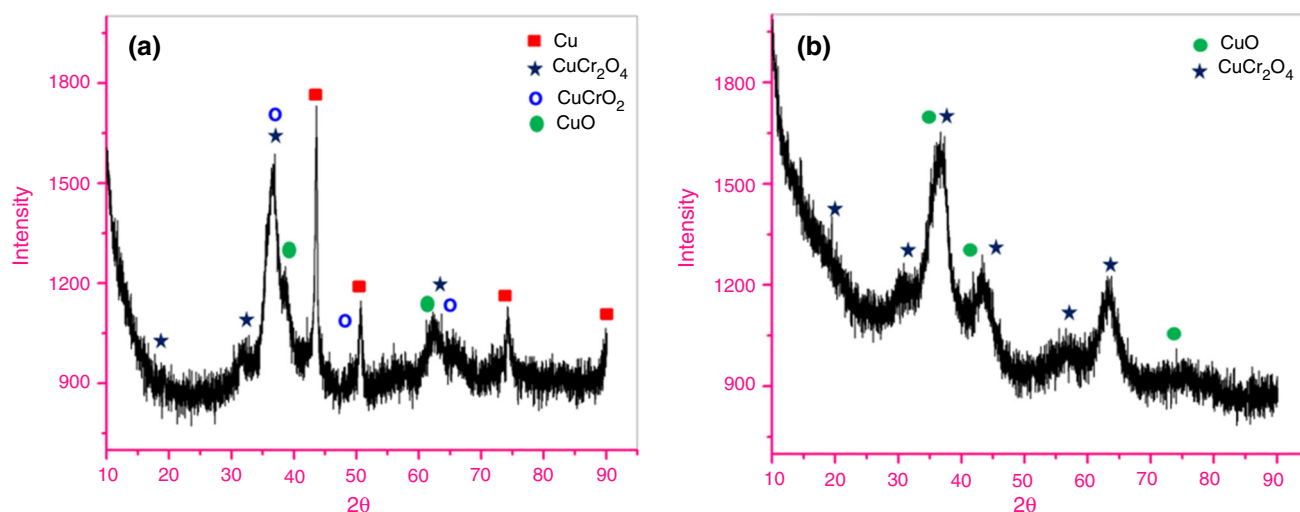
Fig. 4 X-ray diffractograms of CEC and CAC heated at 598 K in nitrogen atmosphere
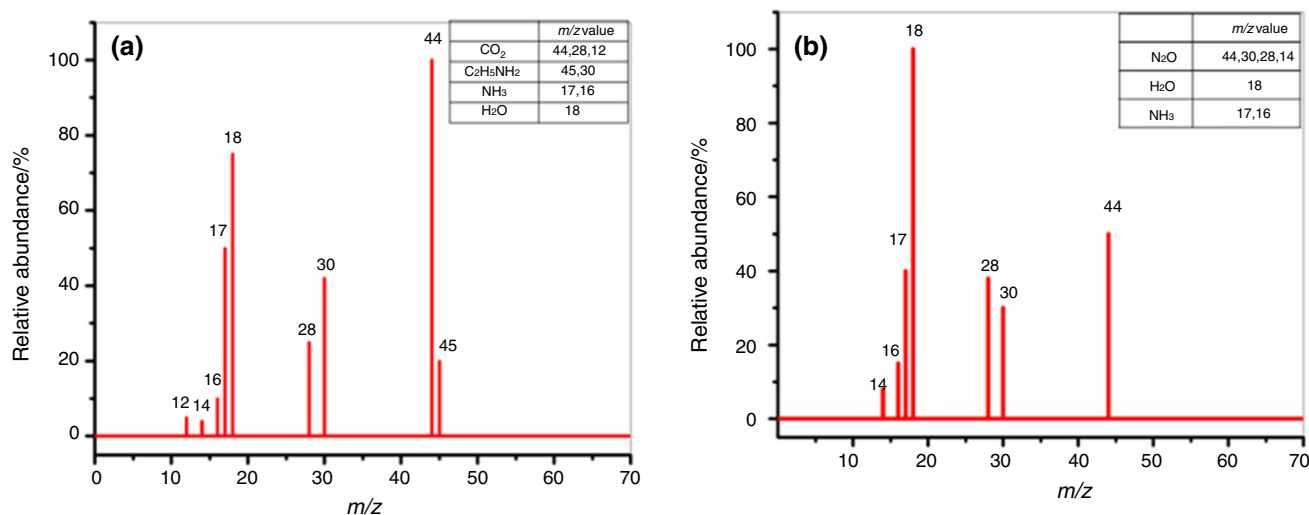
Fig. 5 Mass spectra of first-stage decomposition of CEC and CAC

The second-stage decomposition reaction for both CEC and CAC can be represented as,

$$2CuCrO_4 \rightarrow CuO + CuCr_2O_4 + 1.5O_2. \qquad (14)$$

### Third-stage thermal decomposition (873–973 K)

A third-stage endothermic decomposition was observed in both CEC and CAC from 873 to 973 K accompanied by mass loss of around 2.2 and 3.4 %, respectively (Fig. 1a, b). MS data (Fig. 8) at this stage show the evolution of oxygen during decomposition. This stage is attributed to the solid-state reaction between CuO and $CuCr_2O_4$ to form cuprous chromite ($CuCrO_2$). Independent experiments conducted by us with $CuCr_2O_4$ and CuO showed that the reduction of copper (II) to

copper (I) in these compounds in pure state took place only above 1073 K. This indicates the occurrence of a solid-state reaction between CuO and $CuCr_2O_4$ with the reduction of copper (II) to copper (I) and formation of $CuCrO_2$ and copper (III) oxide (Cr_2O_3) along with the liberation of oxygen during the third-stage decomposition of CEC.
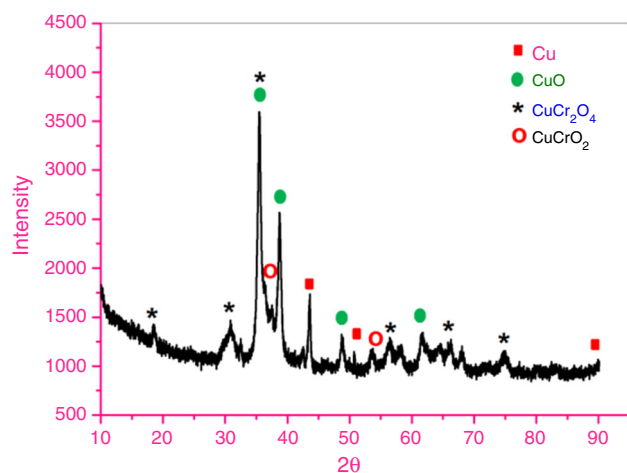
X-ray diffractogram of CEC heated at 973 K in inert atmosphere is shown in Fig. 9, and it shows sharp and intense peaks, indicating the formation of highly crystalline materials. Formation of Cu and $CuCrO_2$ phase during the third-stage decomposition of CEC is confirmed by peaks at 2θ values of 32.5, 35.7, 38.9, 48.7, 53.4, 58.2, 61.4, 65.8 and 82.6 and 31.5, 36.4, 41.0, 56.1, 62.5, 65.8, 71.5, 74.6 and 88.7°, respectively. From XRD, it is inferred that small amount of Cr_2O_3 (JCPDS No.00-038-1479) was also
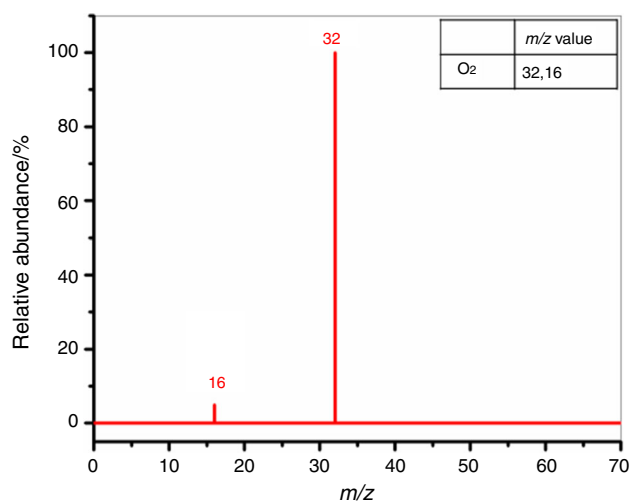
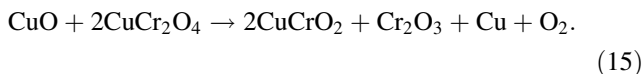**Fig. 6** Mass spectrum of second-stage decomposition of CEC and CAC
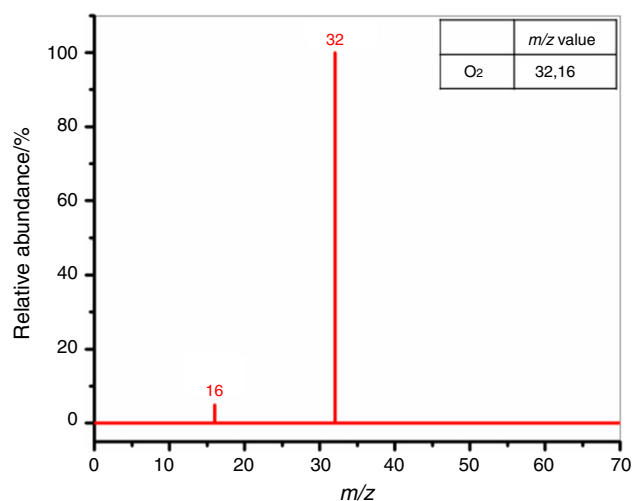
Fig. 8 Mass spectrum of third-stage decomposition of CEC and CAC
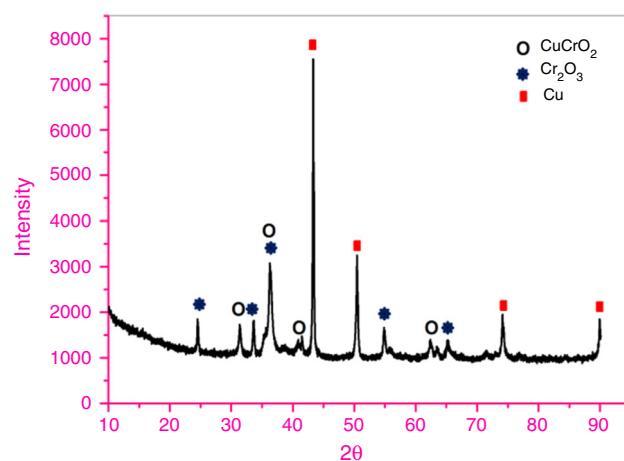

Fig. 7 X-ray diffractogram of CEC heated at 723 K in nitrogen atmosphere

Fig. 9 X-ray diffractogram of CEC heated at 973 K in nitrogen atmosphere

formed during decomposition of CEC. The third-stage decomposition reaction of CEC can be represented as,

$$CuO + 2CuCr_2O_4 \rightarrow 2CuCrO_2 + Cr_2O_3 + Cu + O_2. \quad (15)$$

Fourth-stage thermal decomposition of CEC (1063–1123 K)

CEC alone shows a fourth-stage decomposition from 1063 to 1123 K accompanied by a mass loss of 3 %. Figure 10a, b shows the MS and XRD spectra of the sample heated at 1123 K in nitrogen atmosphere. MS analysis (Fig. 10a) showed an interesting observation that two volatile products, O_2 and CO_2, are liberated at this stage. XRD (Fig. 10b) showed the presence of Cu and Cr_2O_3 only which indicates the reduction of $CuCrO_2$. Evolution of CO_2

(CO_2 at m/z of 44, 28 and 12) during fourth-stage decomposition (Fig. 10a) reveals that the oxygen produced during the previous low-temperature stages is not capable to oxidize the carbon present in the system at that temperature. The reactions taking place during this stage are represented as,

$$2CuCrO_2 \rightarrow 2Cu + Cr_2O_3 + 0.5O_2 \quad (16)$$

$$C + O_2 \rightarrow CO_2. \quad (17)$$
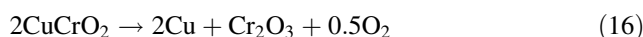
Kinetic parameters for thermal decomposition CEC

The first-stage decomposition of CEC is the major step in the formation of copper chromite catalyst, and hence, it was subjected to detailed kinetic analysis using KAS and
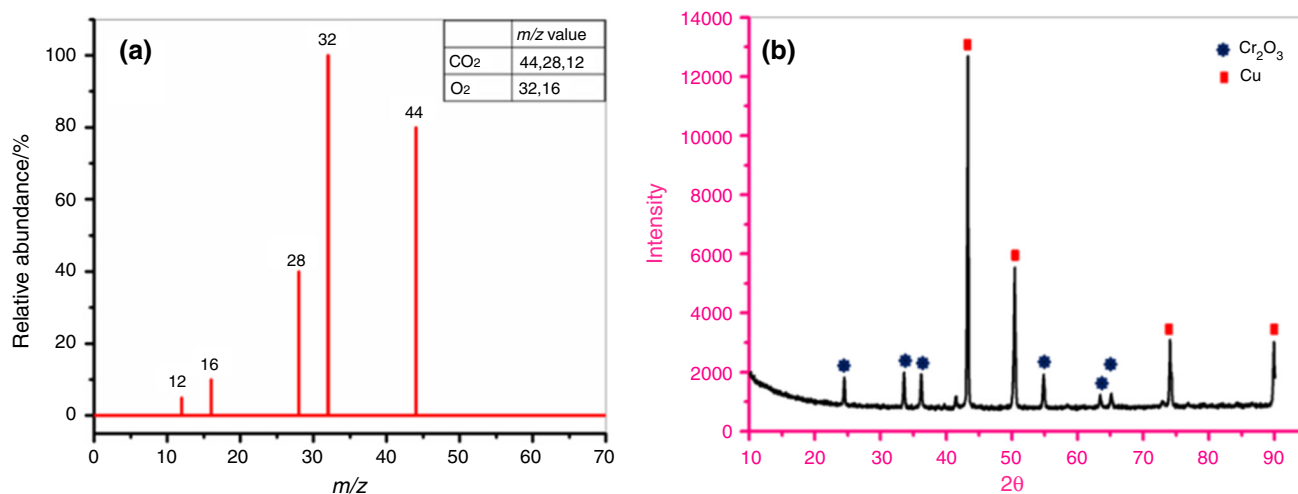
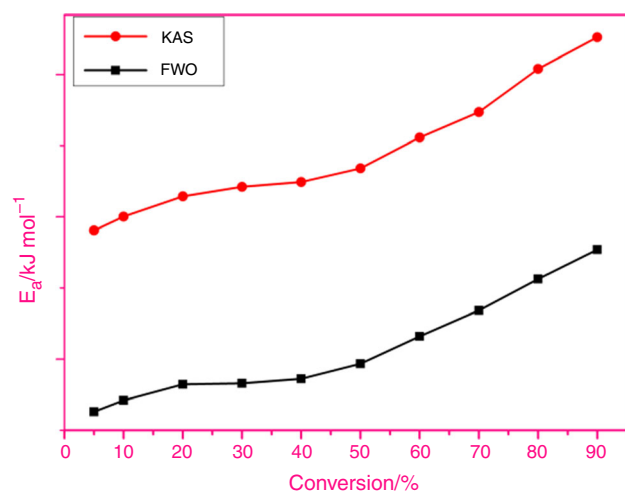**Fig. 10** Mass spectrum and X-ray diffractogram of fourth-stage decomposition of CEC

Fig. 11 Variation of E_a with degree of conversion for CEC using KAS and FWO methods

Table 3 E_a and A values for the thermal decomposition of CEC by KAS and FWO methods

Method	E_a/kJ mol^{-1}	A/min^{-1}
KAS	124.5	3.76×10^{13}
FWO	123.9	3.23×10^{13}

Mechanism of decomposition

The E_a average values obtained using the KAS and FWO methods were used to identify the mechanism of thermal decomposition of CEC from the different mechanisms proposed by Criado [22]. Using Eq. 8, proposed by Coats and Redfern, the activation energy for every $g(\alpha)$ functions listed in Table 1 was calculated from log $g(\alpha)/T^2$ versus $1/T$ plots, where α is the degree of conversion at the temperature T for a heating rate of 10 K min^{-1}. The 13 kinetic plots for CEC are shown in Fig. 12. E_a values obtained from the kinetics plots are given in Table 4. Analysis of Fig. 12 and Table 4 shows that, among the 13 kinetics plots derived for CEC, activation energy corresponding to F1 type mechanism is in good agreement with that obtained using KAS/FWO methods. The process was repeated with thermogravimetric data obtained from experiments with heating rates 5, 20 and 40 K min^{-1} and found that the E_a values obtained from F1 mechanism are 124.5, 125.5 and 122.6 kJ mol^{-1}, respectively, which are in good agreement with that from KAS/FWO methods.

In the F1 mechanism that corresponds to the random nucleation with one nucleus on the individual particle, the decomposition of CEC is initiated from random points that act as growth centre for the development of the decomposition reaction. From TG–MS results for the decomposition of CEC, the decomposition starts with the liberation

FWO methods. The activation energy values obtained by FWO and KAS methods were drawn against the percentage of conversion, ranging from to 5 to 90 %, and are shown in Fig. 11. The average activation energy and pre-exponential factor for CEC by both the methods are given in Table 3.

From Fig. 11 and Table 3, it can be seen that both KAS and FWO methods show comparable kinetic parameters and similar variation with degree of conversion. It can also be seen that E_α values for CEC increase with degree of conversion. This is expected as the decomposition of CEC starts at a lower temperature with the liberation of less stable ethylamine group, followed by its oxidation. As the reaction progresses, oxidation becomes prominent, thereby increasing the overall activation energy. These observations are confirmed by the total ion chromatogram of reaction products shown in Fig. 2a.

Fig. 12 Kinetic curves obtained for CEC with mechanistic equation

Table 4 Activation energy calculated for CEC from different mechanistic equations

	Correlation coefficient	E_a/kJ mol^{-1}
D_1	0.9430	144.7
D_2	0.9644	162.2
D_3	0.9750	7.1
D_4	0.9716	169.5
F_1	0.9983	125.3
F_2	0.7423	58.3
F_3	0.7929	135.0
A_2	0.9808	38.4
A_3	0.9646	19.5
A_4	0.9793	36.3
R_1	0.9239	63.2
R_2	0.9676	77.6
R_3	0.6363	8.81

of ethylamine, and these desorption sites can act as a centre for nucleation. Due to the less stability of the complex, nucleation is started at a lower temperature of around 423 K. This observation is confirmed from the lower E_a value of 124 kJ mol^{-1} (Table 3 and 4) for CEC decomposition than that for CAC [25].

Conclusions

The thermal decomposition of basic copper ethylamine chromate (CEC), precursor for copper chromite catalyst, was followed by hyphenated thermogravimetry–mass spectroscopy and XRD techniques. The results obtained were compared with that of copper ammonium chromate (CAC), the standard precursor for copper chromite. The decomposition of CEC started at a lower temperature and proceeds in four stages. Decomposition products analysed

by TG–MS and XRD showed that first-stage decomposition of CEC took place in a reducing atmosphere, while that of CAC took place in oxidizing atmosphere. The non-volatile products after the first-stage decomposition of CEC were Cu, $CuCr_2O_4$, $CuCrO_2$ and CuO, while those of CAC are $CuCrO_4$ and CuO. Second- and third-stage decompositions were almost similar for both the precursors. These stages correspond to the reduction of $CuCrO_4$ to CuO and $CuCr_2O_4$ and a solid-state reaction between CuO and $CuCr_2O_4$ to form $CuCrO_2$, respectively. CEC showed an additional fourth-stage decomposition corresponding to the reduction of $CuCrO_2$ to Cu, and Cr_2O_3. The kinetic parameters for the first-stage thermal decomposition were derived from thermogravimetric data, and the detailed kinetic analysis showed that the first-stage decomposition of CEC followed F1 mechanism. The E_a values calculated by KAS and FWO isoconversion methods for the first-stage thermal decomposition of CEC show similar variation with the percentage conversion.

References

1. Jacobs PWM, Whitehead MR. Decomposition and combustion of ammonium perchloate. Chemistry. 1969;69:551–90.
2. Zhao F, Chen P, Li S. Effect of ballistic modifiers on thermal decomposition characteristics of RDX/AP/HTPB propellant. Thermochim Acta. 2004;416:75–8.
3. Zhou Z, Tian S, Zeng D, Tang G, Xie C. MOX (M = Zn Co, Fe)/AP shell–core nanocomposites for self-catalytical decomposition of ammonium perchlorate. J Alloys Compd. 2012;513:213–9.
4. Xiao F, Sun X, Wu X, Zhao J, Luo Y. Synthesis and characterization of ferrocenyl-functionalized polyester dendrimers and catalytic performance for thermal decomposition of ammonium perchlorate. J Organomet Chem. 2012;713:96–103.
5. Li W, Cheng H. Cu–Cr–O nanocomposites: synthesis and characterization as catalysts for solid state propellants. Solid State Sci. 2007;9:750–5.
6. Keenan AG, Siegmund RF. Kinetics of the low temperature thermal decomposition of ammonium perchlorate and its catalysis by copper ion. J Solid State Chem. 1972;4:362–9.
7. Kishore K, Sunitha MR. Effect of transition metal oxides on decomposition and deflagration of composite solid propellant systems. AIAAJ. 1979;17(10):1118–25.
8. Prasad R, Singh P. Applications and preparation methods of copper chromite catalysts: a review. Bull Chem React Eng Catal. 2011;6(2):63–113.
9. Patil PR, Krishnamurthy VN, Joshi SS. Effect of nano copper oxide and copper chromite on the thermal decomposition of ammonium perchlorate. Propell Explo Pyrot. 2008;33:4.
10. Gheshlaghi E, Shaabani B, Khodayari Y, Kalandaragh A, Rahimi R. Investigation of the catalytic activity of nano-sized CuO, Co_3O_4 and $CuCo_2O_4$ powders on thermal decomposition of ammonium perchlorate. Powder Technol. 2012;217:330–9.

11. Dubey R, Srivastava P, Kapoor IPS, Singh G. Synthesis, characterization and catalytic behavior of Cu nanoparticles onthe thermal decomposition of AP, HMX, NTO and composite solid propellants, Part 8. Thermochim Acta. 2012;549:102–9.

12. Boldyrev VV. Thermal decomposition of ammonium perchlorate. Thermochim Acta. 2006;443:1–36.

13. Kawamoto AM, Pardini LC, Rezende LC. Synthesis of copper chromite catalyst. Aerosp Sci Technol. 2004;8:591–8.

14. Roy S, Ghose J. 1999 syntheses and studies on some copper chromite spinel oxide composites. Mater Res Bull. 1999;34(7):1179–86.

15. Sanoop AP, Rajeev R, Benny KG. Synthesis and characterization of a novel copper chromite catalyst for the thermal decomposition of ammonium perchlorate. Thermochim Acta. 2015;606:34–40.

16. Tanaka H. Thermal analysis and kinetics of solid state reactions. Thermochim Acta. 1995;267:29–44.

17. Poletto M, Zattera J, Ruth M, Santana C. Thermal decomposition of wood: kinetics and degradation mechanisms. Bioresour Technol. 2012;126:7–12.

18. Boris V, Vov L. Theory of solid-state decomposition reactions: a historical essay. Spectrochim Acta Part B. 2011;66:557–64.

19. Vyazovkin S, Chrissafis K, Lorenzo ML, Koga N, Pijolat M, Roduit B, Sbirrazzuoli N, Sunol JJ. ICTAC Kinetics Committee recommendations for collecting experimental thermal analysis data for kinetic computations. Thermochim Acta. 2014;590:1–23.

20. Akahira T, Sunose T. Method of determining activation deterioration constant of electrical insulating materials. Res Rep Chiba Inst Technol (Sci. Technol). 1971;16:22–31.

21. ASTM E1641 − 13, Standard Test Method for Decomposition Kinetics by Thermogravimetry Using the Ozawa/Flynn/Wall Method. 2013.

22. Criado JM, Malek J, Ortega A. Applicability of the master plots in kinetic analysis of non-isothermal data. Thermochim Acta. 1989;147:377–85.

23. Maqueda LAP, Criado JM, Jimenez PES. Combined kinetic analysis of solid-state reactions: a powerful tool for the simultaneous determination of kinetic parameters and the kinetic model without previous assumptions on the reaction mechanism. J Phys Chem A. 2006;110:12456–62.

24. Patnaik P, Rao DY, Ganguli P, Murthy AS. Decomposition mechanism of copper ammonium chromate: a basic material for copper chromite catalyst. Thermochim Acta. 1983;68:17–25.

25. Rajeev R, Devi KA, Abraham A, Krishnan K, Krishnan TE, Ninan KN, Nair CGR. Thermal decomposition studies: part 19: kinetics and mechanism of thermal decomposition of copper ammonium chromate precursor to copper chromite catalyst and correlation of surface parameters of the catalyst with propellant burning rate. Thermochim Acta. 1995;254:235–47.

26. Hanic F, Horvath I, Plesch G. Study of copper-chromium oxide catalyst. ii. Crystal data and thermal decomposition of basic copper (II) ammonium chromate. Thermochim Acta. 1989;145:19–32.

27. Said AA. The role of copper-chromium oxide catalysts in the thermal decomposition of ammonium perchlorate. J Therm Anal. 1991;37(5):959–67.

28. Habibi M, Fakhri F. Sol–gel combustion synthesis and characterization of nanostructure copper chromite spinel. J Therm Anal Calorim. 2014;115(2):1329–33.

29. Choudhary VR, Pataskar SG. Thermal analysis of ammonium copper chromate. J Therm Anal. 1979;17(1):45–56.

30. Coats AW, Redfern JP. Kinetic parameters from thermogravimetric data. Nature. 1964;201:68–9.